Rare Metal Materials and Engineering
Volume 47, Suppl. 2, August 2018
Cite this article as: Rare Metal Materials and Engineering, 2018, 47(S2): 158-161.

Magnetic Properties of $Mn_{1-x}Zn_xFe_2O_4$ ($0 \leqslant x \leqslant 1$) Nanoparticles Fabricated by a Template-assisted Sol-gel Method

Li Dongyun[1], Sun Yukun[1, 2], Xu Yang[1], Wang Fan[1], Ge Hongliang[1], Yang Hui[2]

[1] China Jiliang University, Hangzhou 310018, China; [2] Zhejiang University, Hangzhou 310027, China

Abstract: A series of Mn-Zn ferrite nanoparticles with a nominal composition $Mn_{1-x}Zn_xFe_2O_4$ ($0 \leq x \leq 1$ with steps of 0.2) were synthesized by a template-assisted sol-gel method. The phase identification and magnetic properties of $Mn_{1-x}Zn_xFe_2O_4$ were measured by XRD and VSM. The effects of Zn content on the structure and magnetic properties of $Mn_{1-x}Zn_xFe_2O_4$ were studied. It is found that all the $Mn_{1-x}Zn_xFe_2O_4$ samples with different Zn contents exhibit cubic spinel structure in single phase. With the increase of Zn content, the values of the crystal plane spacing d, average crystal size D, saturation magnetization M_s, Curie temperature T_c all exhibit a decreasing trend, while, the coercivity H_c shows a first increasing then decreasing trend. For the $Mn_{0.6}Zn_{0.4}Fe_2O_4$ samples, the coercivity H_c is the maximum. The decreasing of M_s is attributed to the Yafet-Kittel canting, the decreasing of T_c is due to the decreasing of anti-ferromagnetic coupling among sublattices. The variation trend of the coercivity H_c can be explained on the basis of the changes of magneto-crystalline anisotropy K_1 of the samples caused by the change of $Mn_{1-x}Zn_xFe_2O_4$ formula with different Zn contents x.

Key words: $Mn_{1-x}Zn_xFe_2O_4$; template-assisted sol-gel; magnetic properties; nano powders

Mn-Zn ferrites have been widely used in many electronic and magnetic fields because of their high magnetic permeability, saturation magnetization, dielectric resistivity and relatively low eddy current losses[1-6]. Mn-Zn ferrites have mixed spinel structure with Fe ions at the tetrahedral site (*A*-site) and octahedral site (B-site), while 80% Mn^{2+} and all Zn^{2+} ions are at the tetrahedral site (*A*-site) and 20% Mn^{2+} ions are at octahedral site (B-site)[7]. Therefore, Mn-Zn ferrites can be represented by the formula $(Zn_xMn_{0.8-0.8x}Fe_{0.2-0.2x})$-$[Mn_{0.2-0.2x}Fe_{1.8+0.2x}]O_4$. The tetrahedral and octahedral sublattice magnetizations of spinel Mn-Zn ferrite materials are antiparallel and therefore a non-compensated magnetic moment occurs resulting in the ferromagnetic structure[8]. Although the Mn-Zn ferrites have mixed spinel structure, the magnetic and electronic properties of these ferrites mainly depend on their chemical composition, method of preparation, grain size, and distribution of cation between two interstitial sites[9]. As is already known, sol-gel technique is feasible for tailoring materials properties by optimizing synthesis parameters (such as the ratio of reaction materials, gelation time/temperature, media pH value). Template-assisted sol-gel synthesis is an effective approach to synthesize chemically homogeneous, size/morphology controllable and high purity nanopowders[10-14].

In this study, $Mn_{1-x}Zn_xFe_2O_4$ nanoparticles ($0 \leq x \leq 1$ with steps of 0.2) were synthesized by a template-assisted sol-gel method. The effects of Zn^{2+} content on lattice structure, crystalline size and magnetic properties of the particles were investigated by X-ray diffraction (XRD) and a vibrating sample magnetometer (VSM).

1 Experiment

$Mn_{1-x}Zn_xFe_2O_4$ (with x=0.0~1.0 with steps of 0.2) powders were prepared by the template-assisted sol-gel method[11]. Iron (III) nitrate nonahydrate, manganese (II) nitrate solution (50%), zinc(II) nitrate hexahydrate, and citric acid, ethanol, and ammonia solution were used for the preparation of the starting sol. The metal nitrates were dissolved in ethanol in required molar ratios to prepare solution A. Citric acid was dissolved in ethanol in a separate vessel to produce solution B. Then solution B was added into solution A. The resulting mixture was stirred for 4 h and then it was quantitatively titrated by an ammonia solution to a pH of 2.1. The obtained sol was stirred for 24 h and then it was absorbed using cotton fibers. Sol absorbed by template was dried in an oven at 353 K to get a Mn-Zn ferrite dry gel. The dry gel was calcined at 1073 K for 1 h and then ground to produce the corresponding ferrite particles.

Received date: August 07, 2017
Foundation item: Zhejiang Science and Technology Planning Project (2015C31041)
Corresponding author: Li Dongyun, Ph. D., Associate Professor, College of Materials Science and Engineering, China Jiliang University, Hangzhou 310018, P. R. China, Tel: 0086-571-87676293, E-mail: lidongyun@cjlu.edu.cn

The phase composition of the as-prepared samples was determined using a Bruker D8 advance X-ray diffractometer with Cu Kα radiation (wavelength λ=0.15418 nm), at a scanning rate of 5°/min and a step of 0.02°. The magnetic properties of the as-prepared samples were measured by a vibrating sample magnetometer (LakeShore7407 VSM) equipped with a 2 Tesla electromagnet at several temperatures in the range from room temperature to 773 K. The saturation magnetization (M_s), coercivity (H_c) and hysteretic losses were evaluated from the magnetic hysteretic loops. Curie temperature (T_c) was determined from the temperature dependence of magnetic moment measured with an applied magnetic field of 1.5 T in 323~773 K range.

2 Result and Discussion

2.1 XRD analysis

Fig.1 shows the XRD patterns of the as-prepared $Mn_{1-x}Zn_xFe_2O_4$ (x=0.0~1.0 with steps of 0.2) samples. XRD patterns of the samples reveal the information of single-phase spinel structure Mn-Zn ferrites. It is found that the (311) peak shifts slightly to a lower degree with the increase of Zn content of $Mn_{1-x}Zn_xFe_2O_4$.

The $d_{(311)}$ interplanar spacing was determined from the position of the (311) peak using the Bragg equation[13],

$$d_{(311)} = \frac{\lambda}{2\sin\theta_{(311)}} \quad (1)$$

Where, θ is the diffraction angle from the position of the (311) peak in the XRD patterns, and λ is the wavelength of X-ray (0.15418 nm).

The average crystal size D was calculated from the (311) peaks in XRD patterns using the Scherrer equation[11,15],

$$D = \frac{k\lambda}{B\sin\theta} \quad (2)$$

Where k is the Scherrer constant (0.89), B is the full width at halt maximum (FWHM) of a diffraction peak, and θ is the diffraction angle from the position of the (311) peak in the XRD patterns.

The calculated interplanar spacing $d_{(311)}$ and the obtained average crystal size values D are reported in Table 1. It is found that the calculated interplanar spacing $d_{(311)}$ of $Mn_{1-x}Zn_xFe_2O_4$ decreased as the Zn content increased which is attributed to the decrease of the average lattice constant a because the ionic radius of Zn^{2+} (0.082 nm) is smaller than that of Mn^{2+} (0.091 nm)[16]. The average crystallite size D evaluated using the Scherer's equation, shows an obvious decrease with the increasing of Zn content. As was already known, the nucleation and growth of crystallites were influenced by the probability of available site for cation occupancy. Compared with Zn^{2+} which only occupies the tetrahedral sites, Mn^{2+} would have a higher probability of available site at octahedral and tetrahedral sites available for each unit cell[17]. Therefore, the Mn^{2+} favors the nucleation process and growth of particles.

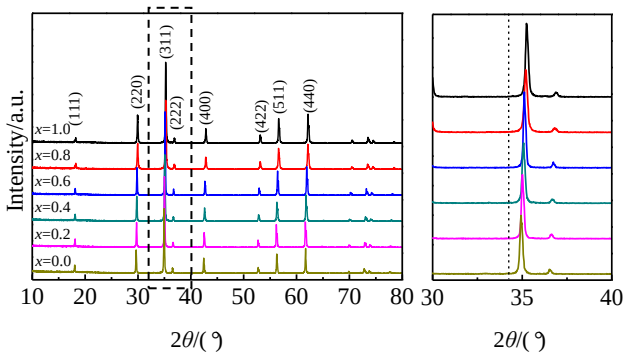

Fig.1 XRD patterns of $Mn_{1-x}Zn_xFe_2O_4$

2.2 Magnetic properties

Fig.2 show the room temperature magnetic hysteresis loops for $Mn_{1-x}Zn_xFe_2O_4$ nano-particles. The magnetic properties of $Mn_{1-x}Zn_xFe_2O_4$ are listed in Table 2. It can be found that the saturation magnetization (M_s) of $Mn_{1-x}Zn_xFe_2O_4$ decreased as Zn content increased which could be explained by changes of the molecular magnetic moments. The similar research results were reported by Hou[18].

The expected cation distributions of $Mn_{1-x}Zn_xFe_2O_4$ according to the occupying rules for the tetrahedral and octahedral sites of Mn and Zn ions are shown in Table 3. The expected saturation magnetization (M_{es}) could be calculated by the following equations[8]:

$$M_s = n \cdot \mu_B \cdot N \quad (3)$$

$$N = \frac{\rho \cdot N_A}{M_W} \quad (4)$$

Table 1 Interplanar spacing $d_{(311)}$ and average crystal size D of $Mn_{1-x}Zn_xFe_2O_4$ (x=0.0~1.0)

Parameter	$Mn_{1-x}Zn_xFe_2O_4$					
	x=0.0	x=0.2	x=0.4	x=0.6	x=0.8	x=1.0
$d_{(311)}$/nm	2.574	2.562	2.557	2.553	2.549	2.545
D/nm	86.1	81.9	76.9	75.8	74.3	72.2

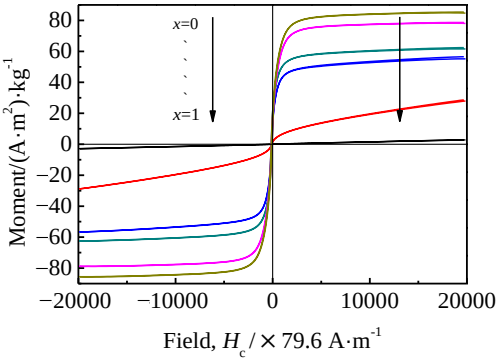

Fig.2 Room-temperature magnetic hysteresis loops for

$Mn_{1-x}Zn_xFe_2O_4$

Table 2 Main magnetic properties of $Mn_{1-x}Zn_xFe_2O_4$

Magnetic property	x=0.0	x=0.2	x=0.4	x=0.6	x=0.8	x=1.0
M_s/(A m^2) kg^{-1}	84.85	78.80	62.47	56.61	27.94	2.86
H_c/×79.6 A m^{-1}	20.40	29.27	39.89	11.70	8.26	7.39

Table 3 Expected cation distributions and saturation magnetization of $Mn_{1-x}Zn_xFe_2O_4$

$Mn_{1-x}Zn_xFe_2O_4$	Cation distribution	n	M_{es}/(A m^2) kg^{-1}
$MnFe_2O_4$	$(Mn_{0.8}Fe_{0.2})^A[Mn_{0.2}Fe_{1.8}]^B$	5	121.08
$Mn_{0.8}Zn_{0.2}Fe_2O_4$	$(Mn_{0.64}Zn_{0.2}Fe_{0.16})^A[Mn_{0.16}Fe_{1.84}]^B$	4	95.99
$Mn_{0.6}Zn_{0.4}Fe_2O_4$	$(Mn_{0.48}Zn_{0.4}Fe_{0.12})^A[Mn_{0.12}Fe_{1.88}]^B$	3	71.35
$Mn_{0.4}Zn_{0.6}Fe_2O_4$	$(Mn_{0.32}Zn_{0.6}Fe_{0.08})^A[Mn_{0.08}Fe_{1.92}]^B$	2	47.35
$Mn_{0.2}Zn_{0.8}Fe_2O_4$	$(Mn_{0.16}Zn_{0.8}Fe_{0.04})^A[Mn_{0.04}Fe_{1.96}]^B$	1	23.37
$ZnFe_2O_4$	$(Zn_{1.0})^A[Fe_{1.0}Fe_{1.0}]^B$	0	0.00

Where n is the magnetic moment per unit formula in Bohr magneton; μ_B is Bohr magneton; N is the amount of formula units per unit volume; ρ was crystal density; N_A is Avogadro constant and M_W is molecular weight. The calculated M_{es} of $Mn_{1-x}Zn_xFe_2O_4$ nano-particles are given in Table 3.

In a unit cell of Mn-Zn ferrite, 20% of Mn was located in the B (octahedral) sites and the rest occupies A (tetrahedral) sites while Zn had strong specific affinity to A (tetrahedral) sites. As Zn doping increased, the A-B exchange turned weaker and B-B sublattice interaction became stronger, which disturbed the parallel arrangement of spin magnetic moments on the B-site and hence Yafet-Kittel canting occurred[18]. The expected saturation magnetization M_{es} of $Mn_{1-x}Zn_xFe_2O_4$ changes as shown in Table 3 are consistent with the results in Fig.2 and Table 2.

It can also be found in Table 2 that H_c values increased first and then decreased with the increasing of Zn content which could be attributed to the changes of magnetic crystal anisotropy constant K_1 caused by the change of Zn content in $Mn_{1-x}Zn_xFe_2O_4$.

The relation curve between Curie temperature T_c and Zn content is shown in Fig.3 (excluding the values of $ZnFe_2O_4$ for its antiferromagnetic properties). It is clear that the Curie

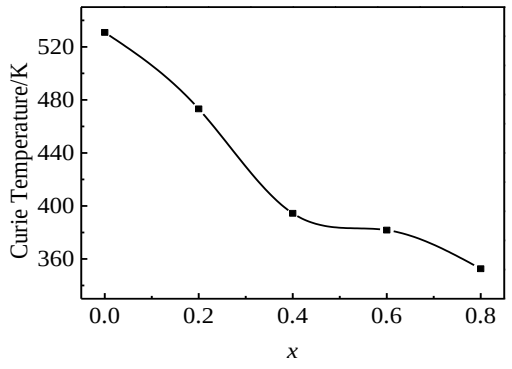

Fig.3 Variation of Curie temperature with Zn concentration x in $Mn_{1-x}Zn_xFe_2O_4$

temperature T_c of $Mn_{1-x}Zn_xFe_2O_4$ decreased as Zn content increased. It is attributed to that the addition of nonmagnetic Zn ions reduced the anti-ferromagnetic coupling among sublattices which means less energy would be needed to destroy the magnetic order in samples[8,16].

3 Conclusions

1) It is found that all the Mn-Zn ferrites with different Zn contents exhibit cubic spinel structure.

2) With the increase of Zn content, the values of the crystal plane spacing d, average crystal size D, saturation magnetization M_s, Curie temperature T_c all exhibit a decreasing trend, while, the coercivity H_c exhibit a first increasing and then decreasing trend. The decreasing of M_s is attributed to the Yafet-Kittel canting, and the decreasing of T_c is due to the decreasing of anti-ferromagnetic coupling among sublattices. The variation trend of the coercivity H_c can be explained on the basis of the changes of magneto-crystalline anisotropy K_1 of the samples caused by the change of $Mn_{1-x}Zn_xFe_2O_4$ formula with different Zn contents x.

References

1 Xing Q K, Peng Z J Wang C B *et al. Physica B: Condensed Matter*[J], 2012, 407: 388
2 Wang W J, Zang C G, Jiao Q G. *Journal of Magnetism and Magnetic Materials*[J], 2014, 349: 116
3 Yang L, Xi G X, Liu J J. *Ceramics International*[J], 2015, 41: 3555
4 Yang W D, Wang Y G. *Journal of Alloys and Compounds*[J], 2015, 625: 291
5 Meng Y Y, Liu Z W, Dai H C *et al*. *Power Technology*[J], 2012, 229: 270
6 Hu P, Yang H B, Pan D *et al. Journal of Magnetism and Magnetic Materials*[J], 2010, 322: 173
7 Jagadeesha A V, Anupama A V, Kumar R *et al. Journal of Alloys and Compounds*[J], 2016, 682: 263
8 Yan Mi, Peng Xiaoling. *Magnetics and Magnetic Materials*[M]. Hangzhou: Zhejiang University Press, 2006 (in Chinese)
9 Hessien M M, Rashad M M, El-Barawy K *et al. Journal of Magnetism and Magnetic Materials*[J], 2008, 320: 1615
10 Sajjia M, Oubaha M, Hasanuzzaman M, Olabi A G. *Ceramics International* [J], 2014, 40(1): 1147
11 Li D Y, Sun Y K, Gao P Z *et al. Ceramics International*[J], 2014, 40(10): 16 529
12 Tangcharoen T, Ruangphanit A, Pecharapa W. *Ceramics International*[J], 2013, 39(1): S239
13 Gabal M A, Elshishtawy R M, Al Angari Y M. *Journal of Magnetism and Magnetic Materials*[J], 2012, 324: 2258
14 Gabal M A, Alluhaibi R S, Alangari Y M. *Journal of Magnetism and Magnetic Materials*[J], 2013, 348: 107

15 Li D Y, Sun Y K, Xu Y *et al. Ceramics International*[J], 2015, 41: 4581
16 Wang Zimin. *Ferrite Production Process Technology*[M]. Beijing: Chemical Industry Press, 2013(in Chinese)
17 Gimenes R, Baldissera M R, dasilva M R A *et al. Ceramics International*[J], 2012, 38: 741
18 Hou X Y, Feng J, Liu X H *et al. Journal of Colloid and Interface Science*[J], 2011, 353(2): 524

$Mn_{1-x}Zn_xFe_2O_4$ ($0 \leqslant x \leqslant 1$) 纳米粉体的模板辅助溶胶凝胶法制备及其磁性能研究

李冬云[1]，孙玉坤[1,2]，徐　扬[1]，王　凡[1]，葛洪良[1]，杨　辉[2]
(1. 中国计量大学，浙江 杭州 310018)
(2. 浙江大学，浙江 杭州 310027)

摘　要：采用模板辅助溶胶-凝胶法制备了一系列的 $Mn_{1-x}Zn_xFe_2O_4$（$0 \leqslant x \leqslant 1$，步长为 0.2）纳米粉体。利用 XRD 和 VSM 对材料的物相和磁性能进行了表征，主要研究了 $Mn_{1-x}Zn_xFe_2O_4$ 分子式中 Zn 含量的变化对样品的微观结构和磁性能的影响。结果表明，具有不同 Zn 含量的 $Mn_{1-x}Zn_xFe_2O_4$ 样品均为尖晶石结构；随着 Zn 含量的增加，样品的晶面间距 d、平均晶粒尺寸 D、饱和磁化强度 M_s 和居里温度 T_c 都呈现出下降的趋势，而样品的矫顽力 H_c 则呈现出先升高后降低的趋势。分析认为，M_s 的下降可以用 Yafet-Kittel 倾角理论解释，T_c 的降低归因于晶格中反铁磁性耦合的降低，而 H_c 的变化则主要是由于材料的磁晶各向异性常数 K_1 的变化引起的。

关键词：$Mn_{1-x}Zn_xFe_2O_4$；模板辅助溶胶凝胶；磁性能；纳米粉体

作者简介：李冬云，女，1972 年生，博士，副教授，中国计量大学材料科学与工程学院，浙江 杭州 310018，电话：0571-87676293，E-mail: lidongyun@cjlu.edu.cn